

Anomaly Machine Component Detection by Deep Generative Model with Unregularized Score

Takashi Matsubara, Ryosuke Tachibana, and Kuniaki Uehara

Graduate School of System Informatics, Kobe University,

1-1 Rokkodai, Nada, Kobe, Hyogo, 657-8501 Japan.

Emails: {matsubara@phoenix., tachibana@ai.cs., uehara@}kobe-u.ac.jp

Abstract—One of the most common needs in manufacturing plants is rejecting products not coincident with the standards as *anomalies*. Accurate and automatic anomaly detection improves product reliability and reduces inspection cost. Probabilistic models have been employed to detect test samples with lower likelihoods as anomalies in unsupervised manner. Recently, a probabilistic model called deep generative model (DGM) has been proposed for end-to-end modeling of natural images and already achieved a certain success. However, anomaly detection of machine components with complicated structures is still challenging because they produce a wide variety of normal image patches with low likelihoods. For overcoming this difficulty, we propose unregularized score for the DGM. As its name implies, the unregularized score is the anomaly score of the DGM without the regularization terms. The unregularized score is robust to the inherent complexity of a sample and has a smaller risk of rejecting a sample appearing less frequently but being coincident with the standards.

I. INTRODUCTION

One of the most common needs in manufacturing plants is rejecting products not coincident with the standards as *anomalies*. Manufacturing companies employ numerous inspectors for the anomaly detection. Accurate and automatic anomaly detection of manufacturing products reduces workloads and inspection cost, and potentially improves product reliability. Especially, anomaly detection based on camera images is attracting attention because it does not require dedicated sensors and can be applied to various products.

Unsupervised anomaly detection is often based on a probabilistic model $p(x)$ of the target domain (see [1] for a survey). The probabilistic model $p(x)$ is constructed with training samples and detects test samples with lower likelihoods as anomalies. Since direct modeling of natural images was troublesome, many studies employed unsupervised methods such as principal component analysis (PCA) to extract features from the images [2]–[6]. Recently, generative models leveraging deep neural networks (DNNs) have been proposed, which are called *deep generative models* (DGMs) [7]–[10]. A DGM can build a generative model of natural images in an end-to-end fashion. The DGM has at least two DNNs called encoder and decoder: The encoder projects a given image onto a lower-dimensional latent space, and the decoder reconstructs the image. Since the DGM learns the data manifold, it keeps frequently appearing images as they were but “repairs” anomaly images as depicted in Fig. 1. Then, the reconstruction error corresponds to a negative log-likelihood and can be treated as

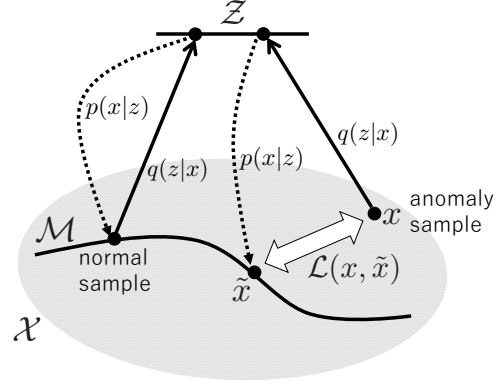


Fig. 1. Data space \mathcal{X} , latent space \mathcal{Z} , and projection by a deep generative model. The encoder $q(z|x)$ projects a sample x in the data space \mathcal{X} onto the latent space \mathcal{Z} . The decoder $p(x|z)$ reconstructs the sample \tilde{x} on the data manifold $\mathcal{M} \subset \mathcal{X}$ from a sample z in the latent space \mathcal{Z} . A normal sample x is on the data manifold \mathcal{M} and is reconstructed successfully. An anomaly sample x is far from the data manifold \mathcal{M} and produces a large reconstruction error $\mathcal{L}(x, \tilde{x})$, which is treated as an anomaly score.

an anomaly score (see [11], Chapter 14, for more detail). The DGM has already achieved a certain success in the task of unsupervised anomaly detection [12]–[17].

However, anomaly detection of machine components with complicated structures is still a challenging problem because of the wide variety of their image patches. Casting products have flat and smooth surfaces but also have curved parts and screw holes. The curved parts and screw holes appear less frequently, resulting in lower likelihoods. Even worse, a screw hole image is inherently more sensitive than a flat surface image to the variability of the production (e.g., the starting point of the screw groove), the imaging direction, and the illumination condition. Difference between normal samples belonging to different classes is larger than that between normal and anomaly samples belonging to the same class. Hence, a probabilistic model has a risk of detecting a normal screw hole as an anomaly instead of a flat surface with a small scratch.

For overcoming this difficulty, we propose *unregularized score* as a novel anomaly score for the DGM [7]. The unregularized score is robust to the inherent complexity of a sample and has a smaller risk of rejecting a sample appearing less frequently but being coincident with the standards. We evaluated the DGMs with the proposed score on our datasets of machine component images and confirmed that they out-

performed their counterparts and conventional approaches by large margins.

II. RELATED WORKS

A. Unsupervised Anomaly Detection

For the practical use in the society, machine learning techniques are desired to learn data with limited expert support. Since the size of accessible data is ever-increasing, manual labeling of the entire samples becomes impossible or too costly. Hence, a practical demand of unsupervised learning arises. Unsupervised anomaly detection has often employed a probabilistic model (see [1] for a survey). A probabilistic model is trained using given training samples and then applied to test samples. Since the training samples are assumed to contain limited or no anomalies, an anomaly test sample has a low probability of being generated from the model. Gaussian mixture model (GMM) is one of generative models used for the anomaly detection [4], [6], [18]. A GMM assumes that each sample x is in the data space $\mathcal{X} \subset \mathbb{R}^{N_x}$ and belongs to one of the hidden classes $z \in \{1, 2, \dots, N_z\}$. Each hidden class z has a multivariate Gaussian distribution as its base distribution. Then, the GMM is expressed as

$$p(x) = \sum_{k=1}^{N_z} w_k p(x|z=k) = \sum_{k=1}^{N_z} w_k \frac{1}{\sqrt{(2\pi)^{N_x} |\Sigma_k|}} \exp\left(-\frac{1}{2}(x-\mu_k)^T \Sigma_k^{-1} (x-\mu_k)\right), \quad (1)$$

where w_k denotes the mixture weight of the hidden class k satisfying $\sum_{k=1}^{N_z} w_k = 1$, and μ_k and Σ_k denote the mean vector and the covariance matrix of the multivariate Gaussian distribution of the hidden class k . The GMM is often trained using the Expectation-Maximization (EM) algorithm. The anomaly score of the GMM is the negative log-likelihood

$$\mathcal{L}_{GMM} = -\log p(x) \quad (2)$$

Since it has been difficult to model natural images directly, many studies employed unsupervised dimension reduction methods such as principal component analysis (PCA), saliency detection, and optical flow to extract features from the images. After that, probabilistic models have been employed to model the extracted features and to detect anomalies [2]–[6], [18].

B. Probabilistic Model on Neural Networks

For leveraging the flexibility of deep neural networks (DNNs), implementation of probabilistic models on DNNs has been investigated, e.g., Boltzmann machine, neural variational inference learning, and generative stochastic network [19]–[21]. Recently, *deep generative model* (DGM) has been proposed as an alternative implementation approach [7]. A DGM can build a model of natural images without feature extractions, i.e., in an end-to-end fashion. It is considered as a more general and robustly trainable model than other DNN-based generative models since it can implement a wide variety of

probabilistic models and is less dependent on Monte Carlo sampling [8]–[10].

We introduce the simplest version of DGMs, i.e., variational autoencoder (VAE) [7]. We consider a probabilistic model $p_\theta(x)$ of a sample x in the data space $\mathcal{X} \subset \mathbb{R}^{N_x}$ with a latent variable z in a latent space $\mathcal{Z} \subset \mathbb{R}^{N_z}$ for $N_z < N_x$;

$$p_\theta(x) = \int_z p_\theta(x|z)p(z), \quad (3)$$

where θ is a set of parameters and $p(z)$ is the prior distribution of the latent variable z . Based on the variational method [22], the model evidence $\log p_\theta(x)$ is bounded using an inference model $q_\phi(z|x)$ parameterized by ϕ as

$$\begin{aligned} \log p_\theta(x) &= \mathbb{E}_{q_\phi(z|x)} \left[\log \frac{p_\theta(x, z)}{p_\theta(z|x)} \right] \\ &= \mathbb{E}_{q_\phi(z|x)} \left[\log \frac{p_\theta(x, z)}{q_\phi(z|x)} \right] + D_{KL}(q_\phi(z|x) || p_\theta(z|x)) \\ &\geq \mathbb{E}_{q_\phi(z|x)} \left[\log \frac{p_\theta(x, z)}{q_\phi(z|x)} \right] \\ &= -D_{KL}(q_\phi(z|x) || p(z)) + \mathbb{E}_{q_\phi(z|x)} [\log p_\theta(x|z)] \\ &=: -\mathcal{L}_{VAE}(x), \end{aligned} \quad (4)$$

where $D_{KL}(\cdot || \cdot)$ is the Kullback-Leibler divergence and $-\mathcal{L}_{VAE}(x)$ is the evidence lower bound. The negative evidence lower bound $\mathcal{L}_{VAE}(x)$ is the objective function to be minimized.

The VAE implements these probabilistic models $p_\theta(x|z)$ and $q_\phi(z|x)$ on DNNs using the *reparameterization trick*. The inference model $q_\phi(z|x)$ is implemented on a DNN called *encoder*. The encoder accepts a data sample x and infers the parameters of the variational posterior $q_\phi(z|x)$ instead of a point estimate of the latent variable z . Then, one can calculate the Kullback-Leibler divergence $D_{KL}(q_\phi(z|x) || p(z))$. The generative model $p_\theta(x|z)$ is also implemented on a DNN called *decoder*. The decoder accepts a latent variable z and then outputs the parameters of the conditional probability $p_\theta(x|z)$ of the data sample x . This also enables one to calculate the conditional log-likelihood $\log p_\theta(x|z)$. The expectation $\mathbb{E}_{q_\phi(z|x)} [\log p_\theta(x|z)]$ is calculated by Monte Carlo sampling from the variational posterior $q_\phi(z|x)$. In the original implementation [7], the latent variable z is sampled once per iteration during the training. In the test phase, the maximum a posteriori (MAP) estimate of the latent variable z (i.e., the mean vector μ_z) is used in place of Monte Carlo sampling. This simplification has been confirmed not to cause serious performance deterioration. For anomaly detection, the VAEs used the evidence lower bound $-\mathcal{L}_{VAE}(x)$ in place of the log-likelihood $\log p_\theta(x)$, i.e., the negative evidence lower bound $\mathcal{L}_{VAE}(x)$ is the anomaly score for the VAE [13], [14].

III. METHODS

A. Unregularized Score for Variational Autoencoder

We propose the *unregularized score* for anomaly detection by the VAE (see also Fig. 2). Following the original study [7], the prior distribution $p(z)$ is set to a standard multivariate

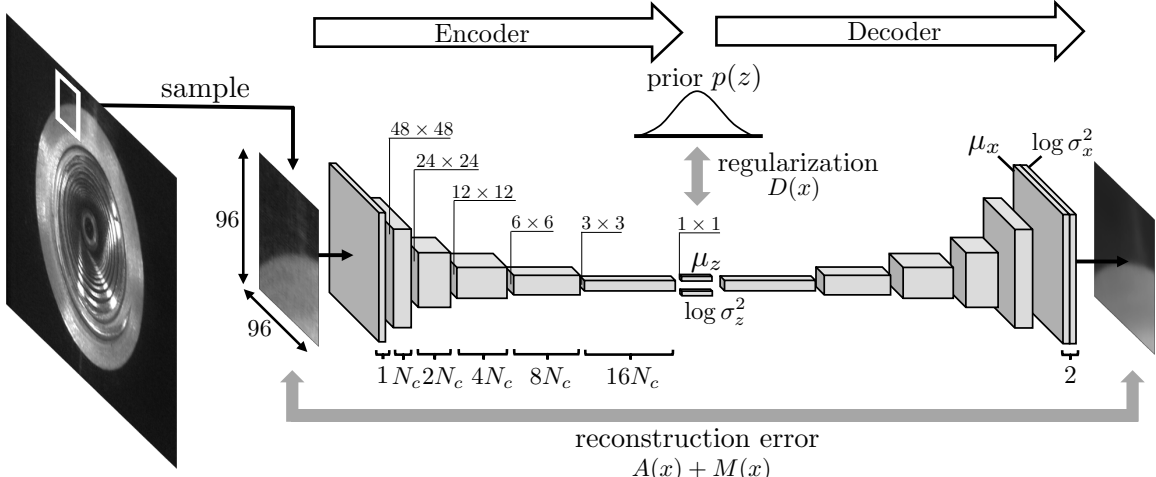


Fig. 2. A diagram of the variational autoencoder (VAE) implemented on the convolutional neural networks (CNNs).

Gaussian distribution. Each of the variational posterior $q_\phi(z|x)$ and the conditional probability $p_\theta(x|z)$ is modeled as a multivariate Gaussian distribution with a diagonal covariance matrix. The output of the encoder is a pair of a mean vector μ_z and a standard deviation vector σ_z of the variational posterior $q_\phi(z|x)$. The output of the decoder is a pair of a mean vector μ_x and a standard deviation vector σ_x of the conditional probability $p_\theta(x|z)$. As described above, the MAP estimate μ_z of the latent variable z is used for the anomaly detection instead of Monte Carlo sampling from the variational posterior $q_\phi(z|x)$. Then, the negative evidence lower bound $\mathcal{L}_{VAE}(x)$ can be rewritten as

$$\begin{aligned} \mathcal{L}_{VAE}(x) &= D_{KL}(q_\phi(z|x)||p(z)) - \log p_\theta(x|\mu_z) \\ &= D_{VAE}(x) + A_{VAE}(x) + M_{VAE}(x) \end{aligned} \quad (5)$$

where

$$\begin{aligned} D_{VAE}(x) &= \sum_{j=1}^{N_z} \frac{1}{2} (-\log \sigma_{z_j}^2 - 1 + \sigma_{z_j}^2 + \mu_{z_j}^2), \\ A_{VAE}(x) &= \sum_{i=1}^{N_x} \frac{1}{2} \log 2\pi \sigma_{x_i}^2 \Big|_{z=\mu_z}, \\ M_{VAE}(x) &= \sum_{i=1}^{N_x} \frac{1}{2} \frac{(\mu_{x_i} - x_i)^2}{\sigma_{x_i}^2} \Big|_{z=\mu_z}, \end{aligned} \quad (6)$$

and i and j denote the indices of the elements related to the sample x and the latent variable z , respectively. From the viewpoint of neural networks, $A_{VAE}(x) + M_{VAE}(x)$ is referred to as a reconstruction error and $D_{VAE}(x)$ is a regularization term. $A_{VAE}(x)$ corresponds to the logarithm of the normalizing constant, which makes the integral of the probability density function of the Gaussian distribution $p_\theta(x|z)$ equal to 1. $M_{VAE}(x)$ is apparently similar to Mahalanobis' distance or normalized Euclidean distance.

Here, we propose an alternative anomaly score

$$\mathcal{L}_{VAE,M}(x) = M_{VAE}(x) \quad (7)$$

in place of the negative evidence lower bound $\mathcal{L}_{VAE}(x) = D_{VAE}(x) + A_{VAE}(x) + M_{VAE}(x)$. Since the log-normalizing constant $A_{VAE}(x)$ and the regularization term $D_{VAE}(x)$ are

removed, we name this score $\mathcal{L}_{VAE,M}$ the *unregularized score*. Note that the objective function of the VAE is still the negative evidence lower bound $\mathcal{L}_{VAE}(x) = D_{VAE}(x) + A_{VAE}(x) + M_{VAE}(x)$.

B. Unregularized Score for Gaussian Mixture Model

For comparison, we also introduce the unregularized score for the GMM. When the hidden class z that a sample x belongs to is determined by the MAP estimate like the VAE, the negative log-likelihood of the sample x is

$$-\log p(x|z=k) = D_{GMM}(x) + A_{GMM}(x) + M_{GMM}(x) \quad (8)$$

where

$$\begin{aligned} D_{GMM}(x) &= -\log w_k, \\ A_{GMM}(x) &= \frac{1}{2} \log (2\pi)^{N_x} |\Sigma_k|, \\ M_{GMM}(x) &= \frac{1}{2} (x - \mu_k)^T \Sigma_k^{-1} (x - \mu_k), \end{aligned} \quad (9)$$

and $k = \arg \max_z p(z|x)$. Then, the unregularized score of the GMM is $\mathcal{L}_{GMM,M} = M_{GMM}(x)$. When the number of the hidden classes N_z of the GMM is set to one, the unregularized score $\mathcal{L}_{GMM,M} = M_{GMM}(x)$ is equivalent to the half of the Mahalanobis' distance $(x - \mu_k)^T \Sigma_k^{-1} (x - \mu_k)$ [1].

C. Concept of Unregularized Score

We consider that the terms $D_{GMM}(x)$, $A_{GMM}(x)$, and $M_{GMM}(x)$ of the GMM correspond to the terms $D_{VAE}(x)$, $A_{VAE}(x)$, and $M_{VAE}(x)$ of the VAE, respectively.

We assume that machine components are composed of a wide variety of subparts such as flat surfaces, curved parts, and screw holes. In this case, the difference between normal samples obtained from different subpart groups is larger than the difference between normal and anomaly samples obtained from the same subpart group as shown in Fig 3. The GMM makes the normal samples from each subpart group to belong to a hidden class, and it makes the anomaly samples to belong not to a specific anomaly class but to the hidden classes that many normal samples also belong to. Under this assumption, the mixture weight w_k represents the frequency

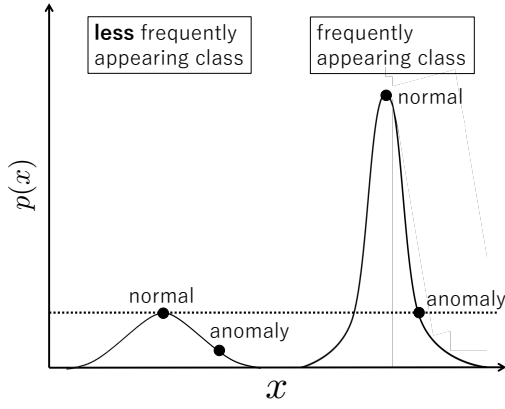


Fig. 3. An intuitive explanation of the unregularized score. The negative log-likelihood of a normal sample obtained from a less frequently appearing class (left) is larger than that of an anomaly sample obtained from a frequently appearing class (right). The negative log-mixture weights $D_{GMM}(x)$ represents the infrequency of the hidden class k and the log-normalizing constants $A_{GMM}(x)$ represents the distribution within the hidden class k . The half Mahalanobis' distance $M_{GMM}(x)$ represents the distance from the center of the distribution of the class k normalized using the covariance matrix Σ_k .

of the corresponding subpart group z and the covariance matrix Σ_k represents the distribution of the samples from the corresponding subpart group z . Hence, the negative log-mixture weight $D_{GMM}(x)$ and the log-normalizing constant $A_{GMM}(x)$ do not work well for the anomaly detection. On the other hand, the half Mahalanobis' distance $M_{GMM}(x)$ represents the distance from the center of the distribution of the class z normalized by the covariance matrix Σ_k . It works as the anomaly score within the class z .

If the VAE is used as an unsupervised feature extractor like the PCA, the latent variable z is treated as an extracted feature [7] and the regularization term $D_{VAE}(x)$ is expected to work as the anomaly score [23]. However, the VAE is usually *undercomplete* (i.e., $N_z < N_x$): It projects a given sample x in the higher-dimensional data space \mathcal{X} to the lower-dimensional latent space \mathcal{Z} . For reconstructing the original sample x , the VAE learns the most salient features in the given samples and ignores less frequently appearing features. When an anomaly sample x_a includes a minor anomaly but is very similar to another normal sample x obtained from the same subpart, the anomaly sample x_a is projected to a position z near the normal sample x . Hence, like the negative log-mixture weight $D_{GMM}(x)$ of the GMM, the regularization term $D_{VAE}(x)$ does not work well for the anomaly detection.

As long as the VAE reconstructs the sample x accurately (i.e., outputs the mean vector μ_x close to x), an appropriate standard deviation σ_x is near-zero, which minimizes the log-normalizing constant $A_{VAE}(x)$. However, if the VAE cannot estimate the appropriate mean vector μ_x , it outputs a large standard deviation σ_x to avoid the normalized distance $M_{VAE}(x)$ exploding. The VAE is trained to balance the two criteria $A_{VAE}(x)$ and $M_{VAE}(x)$ by adjusting the standard deviation σ_x depending on the uncertainty of the reconstruction. This indicates that the log-normalizing constant $A_{VAE}(x)$ has a

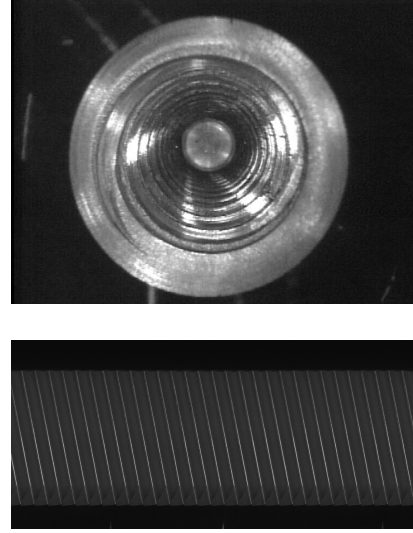


Fig. 4. Example samples in Datasets. (top panel) A sample in the screw dataset. (bottom panel) A sample in the gear dataset.

larger value for a normal sample obtained from a complicated subpart. In other words, the standard deviation σ_{x_i} potentially represents the unpredictability and inherent complexity of the sample x or of the subgroup that the sample x belongs to like the covariance matrix Σ_k of the GMM. Hence, the log-normalizing constant $A_{VAE}(x)$ does not contribute to the anomaly detection.

Only the normalized distance $M_{VAE}(x)$ is directly related to the reconstruction error. Moreover, it is normalized by the standard deviation σ_{x_i} . Hence, the normalized distance $M_{VAE}(x)$ is robust to the unpredictability and inherent complexity of the sample x and is a useful score for the anomaly detection. In the following sections, we will evaluate the VAE with the unregularized score $\mathcal{L}_{vae,M}$ and this concept.

IV. RESULTS

A. Data Acquisition

We evaluated the unregularized score on the image datasets of machine components obtained from production lines owned by AISIN AW CO., LTD. The *screw dataset* is a dataset of 640×480 grayscale images of screw holes (see the top panel of Fig. 4). Each image shows a screw hole at the center and the flat black surface surrounding the screw hole. It also shows camera enclosure at the right and left ends. One of the typical anomalies in the screw dataset is discontinuity such as crack, seam, and porosity, which are caused by entrained gas and shrinkage of the material. The discontinuity deteriorates casting strength and causes troubles by the flakes. Apparently, the image patches of this dataset form two or more clusters; screw grooves, flat surfaces, bottoms of screw holes, and so on. The screw dataset is composed of 12,406 training samples and 995 test samples (including 888 normals and 107 anomalies). The test samples were labeled by experts in AISIN AW CO., LTD. and used for performance evaluation while the training samples were unlabeled and used for parameter adjustment.

TABLE I
THE RESULTANT ROC-AUCs.

Model	Score	Screw Dataset		Gear Dataset	
		Hyper-Parameters	ROC-AUC	Hyper-Parameters	ROC-AUC
Ordinary Anomaly Score					
GMM	\mathcal{L}_{GMM}	$N_h = 200, N_z = 10$	0.637	$N_h = 200, N_z = 100$	0.987
AE	\mathcal{L}_{AE}	$N_c = 32, N_z = 50$	0.719	$N_c = 32, N_z = 20$	0.905
VAE	\mathcal{L}_{VAE}	$N_c = 32, N_z = 20$	0.750	$N_c = 16, N_z = 50$	0.991
Unregularized Score					
GMM	$\mathcal{L}_{GMM,M}$	$N_h = 200, N_z = 20$	0.560	$N_h = 200, N_z = 100$	0.989
VAE	$\mathcal{L}_{VAE,M}$	$N_c = 32, N_z = 20$	0.883	$N_c = 16, N_z = 50$	0.994

The training samples were expected to contain anomalies at the same rate as the test samples. The *gear dataset* is a dataset of $2,200 \times 1,024$ grayscale images of the tooth surfaces of gear wheels (see the bottom panel of Fig. 4). One of the typical anomalies in the gear dataset is casting surface remaining unpolished, which is caused by insufficient adjustment of brushes. It produces undesired friction with other gears. Since the gear teeth are aligned periodically, the image patches of this dataset might not form multiple clusters and then the assumption of the unregularized score depicted in Fig. 3 might not hold. The gear dataset is composed of 2,796 samples (including 2,769 normals and 27 anomalies). Because of the limited number of samples, we used all the samples for training and evaluation: This condition has a risk of overfitting but is not seriously problematic because our evaluation is unsupervised.

B. Models for Comparison

We implemented a VAE depicted in Fig. 2 using PyTorch v0.1.12 [24]. The VAE was trained using training samples randomly cropped to sizes of 96×96 . In the test phase, a test sample was sequentially cropped to the same size with a stride of 16×16 . If the anomaly score of at least one image patch exceeds a threshold, the test sample was considered as an anomaly. We evaluated the proposed unregularized score $\mathcal{L}_{VAE,M} = M_{VAE}(x)$ and the ordinary anomaly score $\mathcal{L}_{VAE} = D_{VAE}(x) + A_{VAE}(x) + M_{VAE}(x)$.

The VAE has an encoder composed of five convolution layers and one fully-connected layer. The n -th convolution layer had a 4×4 kernel and a stride of 2 and outputted a feature map of $N_c \times 2^{n-1}$ channels. Each convolution layer was followed by batch normalization [25] and ReLU activation function [26]. The fully-connected layer outputted $2 \times N_z$ units, followed by the identity function as the activation function. N_z units were used as the mean vector μ_z and the other units were considered to represent $\log \sigma_z^2$. This makes it easier to calculate the Kullback-Leibler divergence $D_{KL}(q_\phi(z|x)||p(z))$. The decoder had a structure paired up with the encoder. The output of the decoder was an image of 2 channels: One was the mean vector μ_x and the other was the standard deviation vector σ_x . The VAE was trained using Adam optimizer [27] with parameters of $\alpha = 10^{-3}$, $\beta_1 = 0.9$, $\beta_2 = 0.999$. A weight decay of 0.9999 was additionally

used for the screw dataset. We selected the number N_c of channels of the first feature map from $N_c \in \{16, 32, 64\}$ and the dimension number N_z of the latent space \mathcal{Z} from $\{2, 5, 10, 20, 50, 100\}$. All the other conditions followed the original study [7] and the previous studies [12]–[17].

For comparison, we also evaluated autoencoder (AE). The AE is a simpler version of the VAE and has been used for the anomaly detection [15], [16]. The AE has an encoder and decoder outputting point estimates of the latent variable z and the reconstruction \tilde{x} , respectively. The objective function and the anomaly score were the mean-squared error between the sample x and the reconstruction \tilde{x} , i.e., $\mathcal{L}_{AE} = \frac{1}{N_x} \sum_{i=1}^{N_x} (x_i - \tilde{x}_i)^2$. In other words, the AE has no need for Monte Carlo sampling, no regularization term $D_{VAE}(x)$, and a constant standard deviation σ_{x_i} . The other conditions were the same as those for the VAE.

We implemented a GMM as a baseline using scikit-learn v0.19.1 [28]. We prepared 100 image patches per training sample and extracted a N_h -dimensional feature from each patch using the PCA. We fitted the GMM of full covariance matrices to the extracted features using the EM algorithm. We selected the number of principal components from $N_h \in \{2, 5, 10, 20, 50, 100, 200, 500\}$ and the number of hidden classes from $N_z \in \{2, 5, 10, 20, 50, 100\}$. Then, we used the negative log-likelihood \mathcal{L}_{GMM} and the unregularized score $\mathcal{L}_{GMM,M} = M_{GMM}(x)$ as the anomaly score.

C. Accuracy of Anomaly Detection

Let TP, TN, FP, and FN denote true positive, true negative, false positive, and false negative, respectively. We used the true positive rate (TPR, or sensitivity) and the false positive rate (FPR, or 1-specificity), defined as

$$\begin{aligned} \text{TPR} &= \text{TP}/(\text{TP} + \text{FN}), \\ \text{FPR} &= \text{FP}/(\text{FP} + \text{TN}). \end{aligned}$$

We plotted the receiver operating characteristic (ROC) curves, which is the relationship between the TPR and FPR with the varying threshold. We calculated the areas under the ROC curves (ROC-AUCs). We summarized the models, the hyper-parameters, and the best ROC-AUCs in Table I. We plotted their ROC curves in Fig. 5. We also summarized the ROC-AUCs of the VAE and AE with the varying dimension number

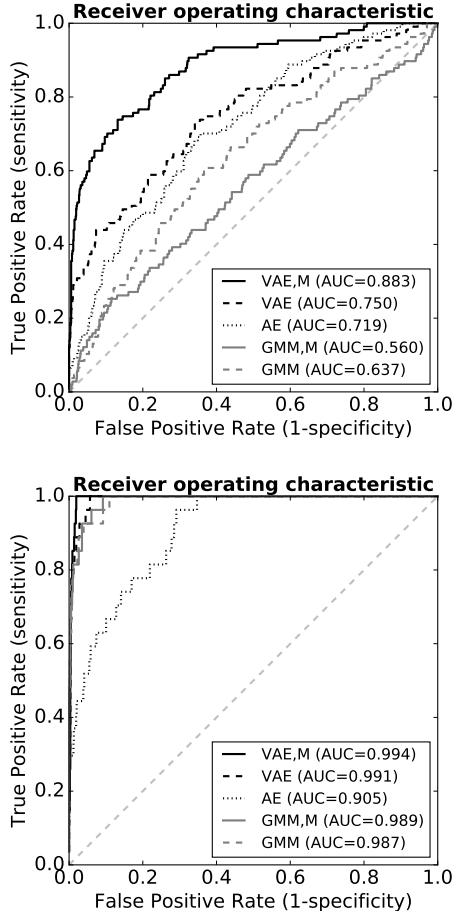


Fig. 5. The receiver operating characteristic (ROC) curves of the models with the best hyper-parameters N_c , N_h , and N_z . (top panel) The screw dataset. (bottom panel) The gear dataset.

N_z of the latent space \mathcal{Z} , and those of the GMM with the varying number N_z of the hidden classes in Fig. 6.

V. DISCUSSION

A. Accuracy of Anomaly Detection

As summarized in Table I, the VAE with the proposed unregularized score $\mathcal{L}_{VAE,M}$ outperformed the VAE, the AE, and the GMM. Especially, the VAE with the proposed unregularized score $\mathcal{L}_{VAE,M}$ outperformed its counterpart in both datasets. In the screw dataset, when the dimension number N_z of the latent space was set to a small value such as 2 and 5 or a large value such as 100, the ROC-AUCs of the VAE with the unregularized score $\mathcal{L}_{VAE,M}$ were slightly reduced but still better than the VAE with the ordinary anomaly score \mathcal{L}_{VAE} . In the gear dataset, despite the concern that the assumption in Section III-C might not hold, the proposed unregularized scores did not degrade the performances. The GMM with the proposed unregularized score $\mathcal{L}_{GMM,M}$ outperformed its counterpart in the gear dataset but not in the screw dataset.

B. Visualization of Anomaly Scores

We visualized an example screw hole and the ground truth of anomaly areas in Fig. 7. One can find the cracks (blowholes

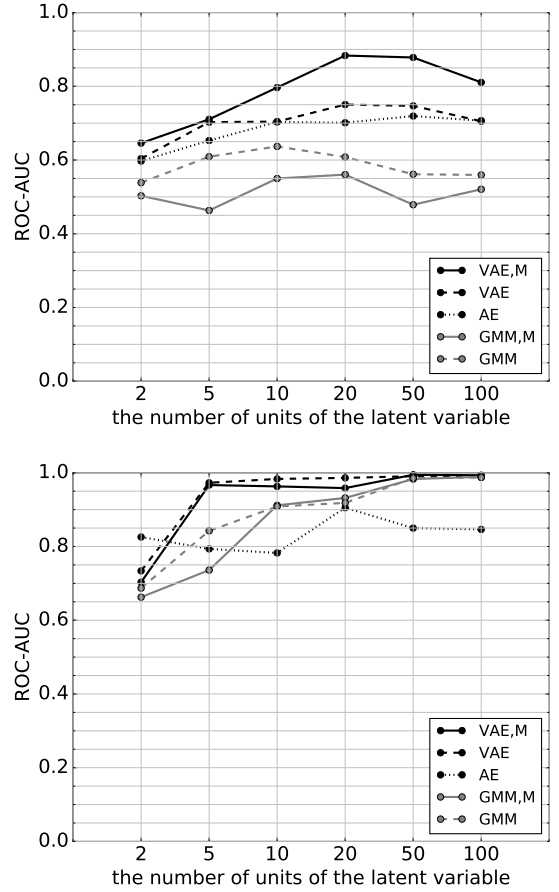


Fig. 6. The areas under the ROC curves (ROC-AUCs) of the VAE and AE with the varying dimension N_z of the latent space \mathcal{Z} , and those of the GMM with the varying number N_z of the hidden classes. (top panel) The screw dataset. (bottom panel) The gear dataset.

in technical terms) at the lower right part of the outermost screw groove and the right part of the middle screw groove as depicted in the top right panel. We also visualized the anomaly scores with a stride of 4×4 , where a brighter pixel represents a lower score.

The anomaly score $\mathcal{L}_{AE}(x)$ of the AE has large values in the anomaly area but also in the screw groove area reflecting the illumination light. Since the AE has a constant standard deviation σ_{x_i} , it is sensitive to pixel intensities more than semantic anomalies.

We first focus on the areas where no anomaly is found. The ordinary anomaly score $\mathcal{L}_{VAE}(x)$ of the VAE have smaller values in the flat black surface area surrounding the screw hole and in the bottom area of the screw hole while they have larger values in the screw groove area despite the fact that these areas are coincident with the standards. This result is not surprising because the image patches from the screw grooves have more variations depending on the relative positions of the image patches and the starting points of the screw grooves. They are more sensitive to the imaging direction and the illumination condition than the image patches from the flat areas. Hence, the likelihood of each image patch from the screw groove

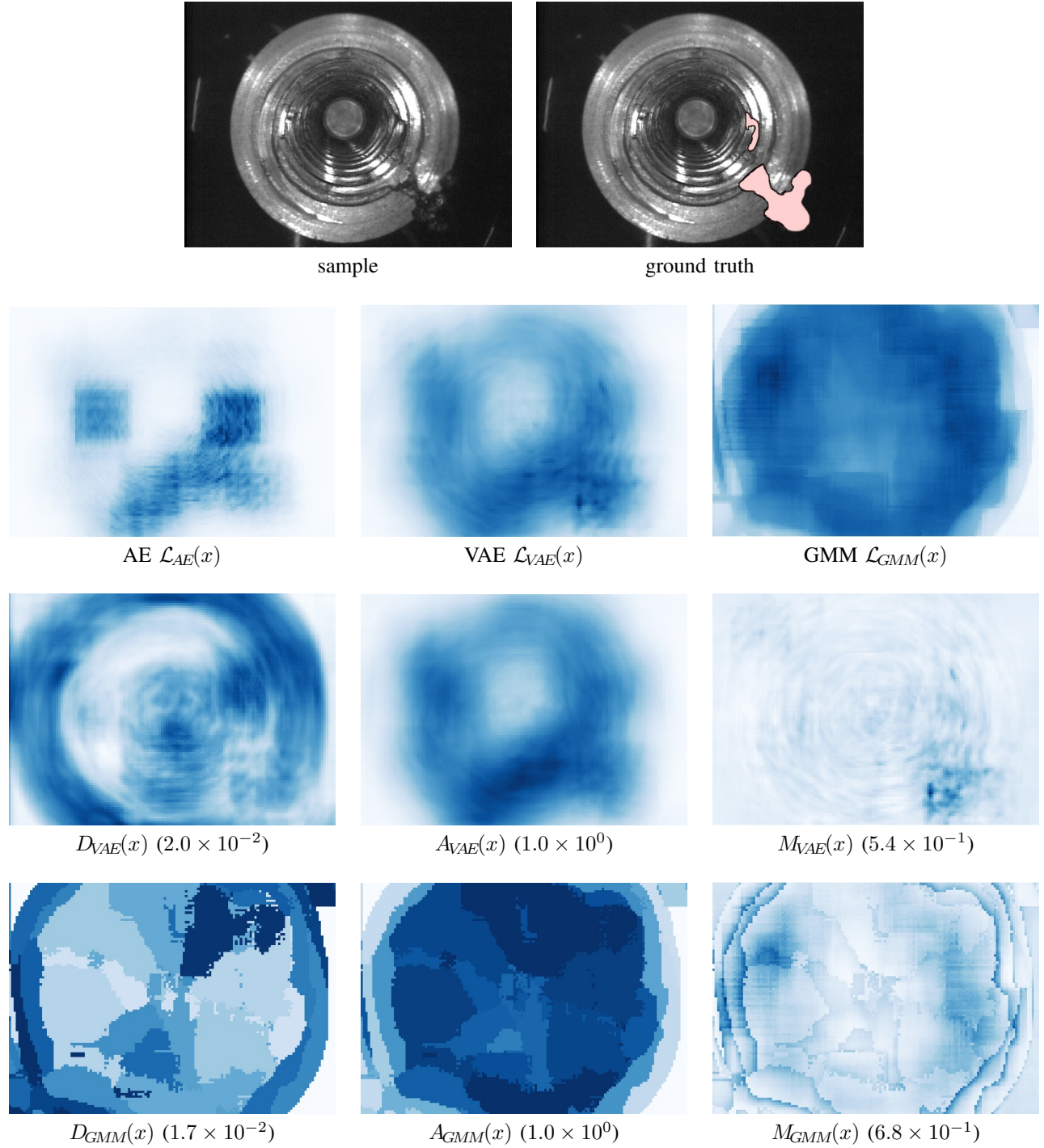


Fig. 7. An example anomaly screw hole, the ground truth of anomaly areas, and the corresponding heat maps of anomaly scores. The anomaly scores were normalized to the range of $[0, 1]$. The relative anomaly scores of the VAE and the GMM can be obtained with the multipliers in parentheses.

areas is naturally lower. In other words, the ordinary anomaly score $\mathcal{L}_{VAE}(x)$ are related to the complexity of the target areas rather than the anomaly as expected in Section III-C. The log-normalizing constant $A_{VAE}(x)$ shows the same tendency since it has a primary effect on the ordinary anomaly score $\mathcal{L}_{VAE}(x)$. The regularization term $D_{VAE}(x)$ shows an opposite tendency, but its value is almost negligible compared to the other terms $A_{VAE}(x)$ and $M_{VAE}(x)$. On the other hand, the normalized distance $M_{VAE}(x)$ is almost constant regardless of the areas where the image patches come from as long as the areas are normal. The absolute error $|x - \mu_x|$ is large in the screw groove areas, but the normalized distance $M_{VAE}(x)$ is normalized by the standard deviation σ_x , which is related to the complexity of the target areas like the log-normalizing constant $A_{VAE}(x)$. As a result, the normalized distance $M_{VAE}(x)$ is robust to the complexity of the target areas. Moreover, for essentially the same reason, only the normalized distance $M_{VAE}(x)$ has obviously large values in the anomaly area. Therefore, the proposed unregularized scores $\mathcal{L}_{VAE,M} = M_{VAE}(x)$ improves the accuracy of the anomaly detection of the machine components with complicated structures.

The ordinary anomaly score $\mathcal{L}_{GMM}(x)$ of the GMM shows that the GMM is insensitive to the anomaly. The GMM parcelled an image into a finite number of classes as shown by the terms $D_{GMM}(x)$ and $A_{GMM}(x)$. Indeed the half Mahalanobis' distance $M_{GMM}(x)$ detects the anomaly modestly as expected, but it is more sensitive to the boundary areas between the classes. This is why the GMM with the unregularized score did not outperform the ordinary GMM.

VI. CONCLUSION

This study proposed the unregularized score of variational autoencoder for the anomaly detection. As its name implies, the unregularized score is the objective function of a generative model without the regularization term. The variational autoencoder with the unregularized score was more robust to image patches obtained from machine components with complicated structures and outperformed its counterparts. Moreover, the unregularized score worked well even for simple structures. Toy datasets and datasets of other machine components will be explored in future work.

ACKNOWLEDGMENT

The authors would like to thank the collaborators from AISIN AW CO., LTD. for insightful suggestions about the image data. This study partially supported by AISIN AW CO., LTD. and the MIC/SCOPE #172107101.

REFERENCES

- [1] V. Chandola, A. Banerjee, and V. Kumar, "Anomaly detection," *ACM Computing Surveys*, vol. 41, no. 3, pp. 1–58, 2009.
- [2] Jaechul Kim and K. Grauman, "Observe locally, infer globally: A space-time MRF for detecting abnormal activities with incremental updates," in *IEEE Conference on Computer Vision and Pattern Recognition (CVPR)*. IEEE, 2009, pp. 2921–2928.
- [3] V. Mahadevan *et al.*, "Anomaly detection in crowded scenes," *IEEE Conference on Computer Vision and Pattern Recognition (CVPR)*, pp. 1975–1981, 2010.
- [4] V. Saligrama and Z. Chen, "Video anomaly detection based on local statistical aggregates," *IEEE Computer Society Conference on Computer Vision and Pattern Recognition (CVPR)*, pp. 2112–2119, 2012.
- [5] M. J. V. Leach, E. P. Sparks, and N. M. Robertson, "Contextual anomaly detection in crowded surveillance scenes," *Pattern Recognition Letters*, vol. 44, pp. 71–79, 2014.
- [6] S. Li, C. Liu, and Y. Yang, "Anomaly Detection Based on Maximum a Posteriori," *Pattern Recognition Letters*, 2017.
- [7] D. P. Kingma and M. Welling, "Auto-Encoding Variational Bayes," *International Conference on Learning Representations (ICLR)*, pp. 1–14, 2014.
- [8] D. P. Kingma, D. J. Rezende, and M. Welling, "Semi-supervised Learning with Deep Generative Models," in *Advances In Neural Information Processing Systems (NIPS)*, 2014, pp. 3581–3589.
- [9] K. Sohn, H. Lee, and X. Yan, "Learning Structured Output Representation using Deep Conditional Generative Models," in *Advances In Neural Information Processing Systems (NIPS)*, 2015, pp. 3483–3491.
- [10] L. Maaløe *et al.*, "Auxiliary Deep Generative Models," in *International Conference on Machine Learning (ICML)*, vol. 48, 2015, pp. 1445–1453.
- [11] I. Goodfellow, Y. Bengio, and A. Courville, *Deep Learning*. The MIT Press, 2016.
- [12] S. Zhai *et al.*, "Deep Structured Energy Based Models for Anomaly Detection," *International Conference on Machine Learning (ICML)*, vol. 48, pp. 1100–1109, 2016.
- [13] S. Suh *et al.*, "Echo-state conditional variational autoencoder for anomaly detection," *International Joint Conference on Neural Networks*, pp. 1015–1022, 2016.
- [14] M. Lopez-Martin *et al.*, "Conditional Variational Autoencoder for Prediction and Feature Recovery Applied to Intrusion Detection in IoT," *Sensors*, vol. 17, no. 9, p. 1967, 2017.
- [15] R. Chalapathy, A. K. Menon, and S. Chawla, "Robust, Deep and Inductive Anomaly Detection," *European Conference on Machine Learning and Principles and Practice of Knowledge Discovery in Databases (ECML-PKDD)*, pp. 1–16, 2017.
- [16] C. Zhou and R. C. Paffenroth, "Anomaly Detection with Robust Deep Autoencoders," *ACM SIGKDD Conference on Knowledge Discovery and Data Mining (KDD)*, pp. 665–674, 2017.
- [17] M. Ribeiro, A. E. Lazzaretti, and H. S. Lopes, "A study of deep convolutional auto-encoders for anomaly detection in videos," *Pattern Recognition Letters*, 2017.
- [18] T. Lu *et al.*, "Anomaly detection through spatio-temporal context modeling in crowded scenes," *International Conference on Pattern Recognition (ICPR)*, pp. 2203–2208, 2014.
- [19] G. E. Hinton, "Boltzmann machine," *Scholarpedia*, vol. 2, no. 5, p. 1668, 2007.
- [20] A. Mnih and K. Gregor, "Neural Variational Inference and Learning in Belief Networks," in *International Conference on Machine Learning (ICML)*, vol. 32, 2014, pp. 1791–1799.
- [21] Y. Bengio *et al.*, "Deep Generative Stochastic Networks Trainable by Backprop," *International Conference on Machine Learning (ICML)*, pp. 226–234, 2013.
- [22] K. Murphy, *Machine Learning: A Probabilistic Perspective*. The MIT Press, 2012.
- [23] T. Schlegl *et al.*, "Unsupervised Anomaly Detection with Marker Discovery," in *Information Processing in Medical Imaging (IPMI)*, 2017, pp. 146–157.
- [24] A. Paszke *et al.*, "Automatic differentiation in PyTorch," in *Autodiff Workshop on Advances in Neural Information Processing Systems*, 2017, pp. 1–4.
- [25] S. Ioffe and C. Szegedy, "Batch Normalization: Accelerating Deep Network Training by Reducing Internal Covariate Shift," in *International Conference on Machine Learning (ICML)*, 2015.
- [26] V. Nair and G. E. Hinton, "Rectified Linear Units Improve Restricted Boltzmann Machines," in *International Conference on Machine Learning (ICML)*, 2010, pp. 807–814.
- [27] D. P. Kingma and J. Ba, "Adam: A Method for Stochastic Optimization," *International Conference on Learning Representations (ICLR)*, pp. 1–15, 2015.
- [28] F. Pedregosa *et al.*, "Scikit-learn: Machine Learning in Python," *Journal of Machine Learning Research*, vol. 12, pp. 2825–2830, 2012.